Revista Internacional de Métodos Numéricos para Cálculo y Diseño en Ingeniería

https://doi.org/10.32604/rimni.2026.082297

ARTICLE

Rainfall Trend Analysis and One-Dimensional Hydrodynamic Assessment of the Ganga River Basin Using HEC-RAS 6.3

Ghritartha Goswami[1], Majed Alsubih[2], Saiful Islam[2], Sudip Basack[3,*] and Pranjit Borah[4]

[1]Hydro Informatics Unit, Water Resources Department, Guwahati, Assam, India
[2]Civil Engineering Department, College of Engineering, King Khalid University, Abha, Saudi Arabia
[3]Department of Civil Engineering, Graphic Era Deemed to be University, Dehradun, Uttarakhand, India
[4]Department of Civil Engineering, North Eastern Regional Institute of Science & Technology, Nirjuli, Arunachal Pradesh, India
*Corresponding Author: Sudip Basack. Email: drsbasack@gmail.com

Received: 13 March 2026; Accepted: 01 June 2026

ABSTRACT: This study integrates long-term rainfall trend analysis with one-dimensional hydrodynamic modelling to assess hydro-climatic variability and flood vulnerability along the selected stretch of the Ganga River near Farakka Barrage, eastern India. Daily gridded rainfall data for 1991–2025 were analyzed to identify trends and potential change points. The Mann–Kendall test, Sen's slope estimator, Bias-Corrected Pre-Whitening, and Trend-Free Pre-Whitening were applied to account for serial correlation. The rainfall series showed an overall decreasing tendency, although statistical significance varied among the applied trend tests after pre-whitening. HEC-RAS 6.3 simulations showed increasing water surface elevation, velocity, and discharge under 25-, 50-, and 100-year design-flood scenarios. The findings indicate that flood risk in the study reach is shaped by both hydro-climatic variability and local hydraulic controls.

KEYWORDS: Rainfall trend analysis; hydrodynamic modelling; ganga river; HEC-RAS; flood risk assessment

1 Introduction

Rainfall variability strongly influences groundwater recharge, river discharge, water availability, and flood or drought risk. Therefore, long-term rainfall trend analysis is essential for water-resource planning under changing climatic conditions [1, 2]. Climate change has altered precipitation regimes and intensified hydrological variability worldwide [3, 4]. Anthropogenic activities, particularly greenhouse gas emissions, have intensified the hydrological cycle, leading to more erratic and extreme rainfall events [5]. In India, many river basins are witnessing an increase in peak annual rainfall, contributing to both flood hazards and water management challenges [6]. These fluctuations not only affect surface runoff and groundwater levels but also alter surface and subsurface flow regimes [7]. The Ganaga River Basin in West Bengal exemplifies these concerns, with increasing frequency and intensity of extreme rainfall events significantly impacting floodplain dynamics, sediment transport, and water supply. Recurrent post-monsoon flooding has affected agricultural productivity, infrastructure, and urban settlements along the river. Furthermore, dry season low-flow conditions challenge irrigation systems and domestic water availability [8]. Despite these pressing issues, comprehensive assessments linking rainfall variability to hydrodynamic responses in the Ganga Basin remain limited. The role of anthropogenic interventions, such as land use change and river regulation, in modifying natural rainfall-runoff relationships also requires further investigation.

Complementing this climatological analysis, the study also explores the hydrodynamic behaviour of the Ganga River Basin using the one-dimensional HEC-RAS 6.3 model. Hydrodynamic modelling examines water movement and flow interaction with channel and floodplain geometry [9]. It has broad applications in rivers and canals, including evaluating climate impacts, river engineering interventions, and flood forecasting [10]. In the context of Indian river basins, flood vulnerability often stems from complex flow patterns and frequent shifts in channel geometry [11-13]. While several rivers in India have been modelled using one- and two-dimensional analyses, fewer studies have focused specifically on the Ganga River Downstream of Farakka Barrage, a critical distributary of the Ganga River originating at the Farakka Barrage in West Bengal [14, 15].

The Ganga, originating from the Gangotri Glacier, is partly diverted at Farakka, where approximately 50% of its discharge enters the Hooghly River. The remaining volume flows into Bangladesh as the Padma River. Both eventually drain into the Bay of Bengal. The Ganga River experiences significant discharge fluctuations and flood risks, especially during the post-monsoon period [8]. These recurring flood events necessitate detailed hydrodynamic assessments to understand flow behaviour and vulnerability under different return period scenarios [16].

To address these gaps, this study integrates rainfall trend analysis with one-dimensional hydrodynamic modelling to assess hydro-climatic variability and flood susceptibility along the Ganga River near Farakka barrage. Recent studies have applied non-parametric methods such as Mann–Kendall and Sen's slope to assess precipitation variability in Indian and South Asian contexts [17- 19]. Here, long-term rainfall trends are evaluated using IMD rainfall data, Mann–Kendall testing, Sen's slope estimation, pre-whitening, modified Mann–Kendall approaches, Pettitt's test [20], and Sequential Mann–Kendall analysis. HEC-RAS 6.3 is then used to simulate water surface elevation, velocity, and discharge under 25-, 50-, and 100-year return-period scenarios. The integrated framework supports flood-risk assessment, infrastructure planning, and disaster preparedness in the Ganga River Basin downstream of Farakka.

2 Study Area

The study area is located near Farakka, West Bengal, India, at approximately 24.80° N and 87.91° E (Fig. 1). The area is important for agriculture and hydropower generation associated with the Farakka Barrage, which is about 2.3 km long, with a 42 km feeder canal [14]. The vulnerable floodplain includes agricultural land, riverine settlements, transport corridors, and local infrastructure. Low-lying fields and densely settled riverbanks increase exposure to inundation, bank erosion, and embankment-related hazards during high-flow events [8].

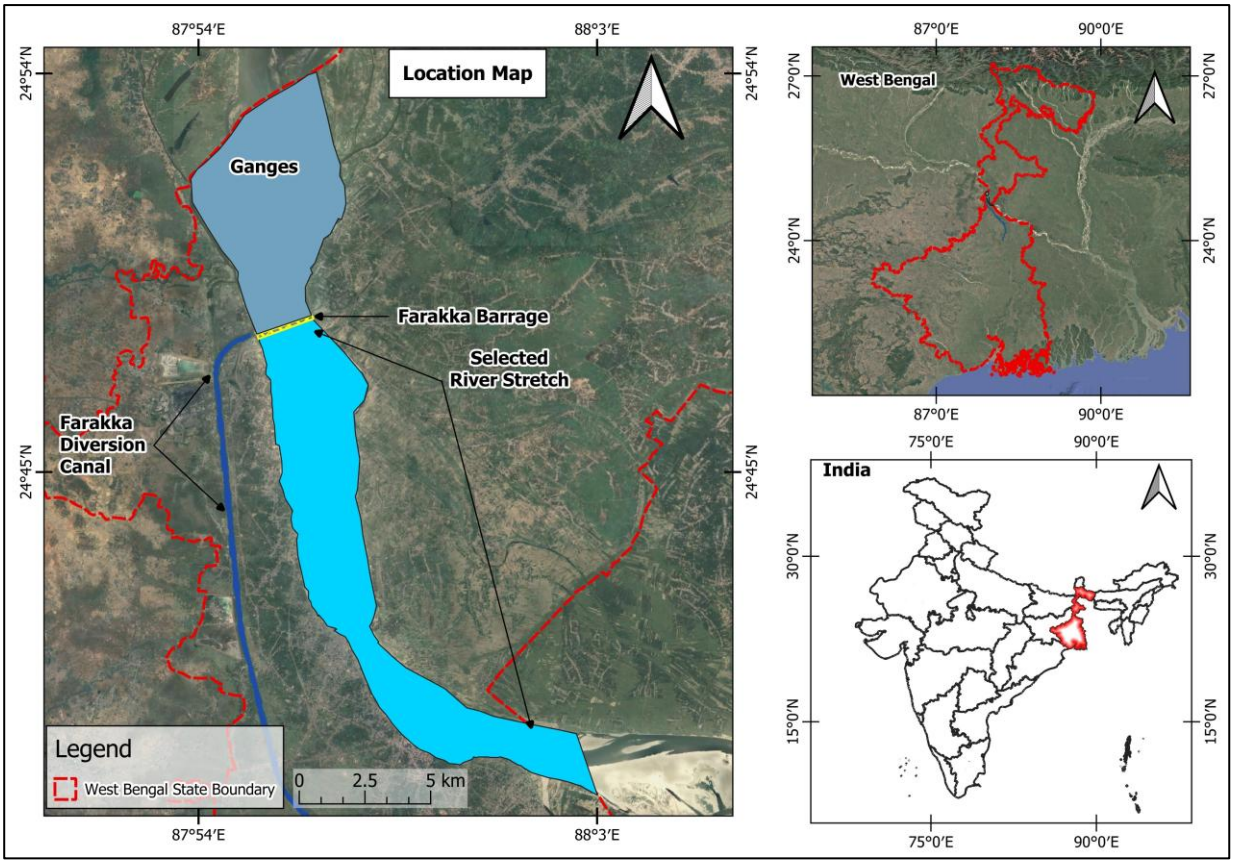

Figure 1: Location of the study area (modified after Goswami et al. 2023a).

3 Methodology

Methodological Overview

The methodology comprised six components: rainfall data preparation, serial-correlation diagnostics, initial trend testing, pre-whitening and modified trend testing, change-point detection, and one-dimensional hydrodynamic simulation using HEC-RAS 6.3. The statistical rainfall analysis and hydrodynamic modelling were conducted as complementary components and were integrated during interpretation. The overall workflow is presented in Fig. 2.

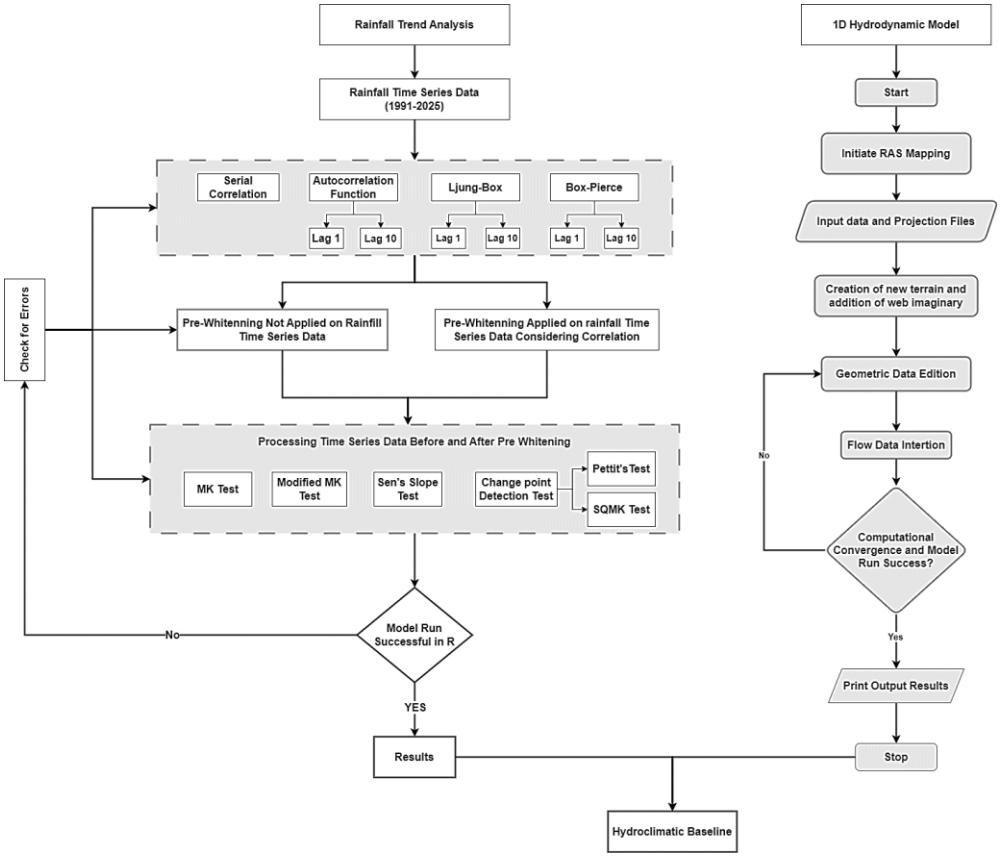

Figure 2: Flowchart for rainfall trend analysis.

Daily rainfall data for 1991–2025 were obtained from the India Meteorological Department (IMD), Pune. The dataset had daily temporal resolution; annual rainfall series were derived from the daily records for long-term trend analysis. The dataset had a spatial resolution of 0.25° × 0.25°, and grid cells covering the study area were extracted and averaged to obtain the representative rainfall series. Annual average rainfall was selected because the objective was to examine long-term hydro-climatic tendency rather than individual storm-event behaviour. ACF was used to identify the magnitude and direction of autocorrelation at selected lags, while Ljung–Box and Box–Pierce tests were applied as portmanteau tests to assess whether serial dependence remained statistically significant. All statistical tests were evaluated at the 5% significance level ($\alpha = 0.05$).

In the first phase, the original rainfall time series was analysed without pre-whitening. The Mann–Kendall test was used to detect monotonic trends, while Sen's slope estimator quantified the magnitude and direction of change. This phase provided a baseline trend estimate before accounting for the possible influence of serial correlation.

In the second phase, serial-correlation correction methods were applied separately rather than simultaneously. Bias-Corrected Pre-Whitening, Trend-Free Pre-Whitening, and modified Mann–Kendall variance-correction approaches were used as alternative treatments to evaluate the sensitivity of trend detection to autocorrelation. Comparing these approaches helped identify whether the trend conclusion was robust or dependent on a particular correction method.

A one-dimensional hydrodynamic analysis was conducted using HEC-RAS 6.3, developed by the U.S. Army Corps of Engineers (USACE 2024). HEC-RAS applies the Saint-Venant equations to simulate water surface elevation, velocity, and discharge along user-defined cross-sections using an implicit finite-difference scheme [21]. The governing continuity and momentum equations used in HEC-RAS are given in Eqs. (1) and (2) [22].

$$\nabla_t A + \nabla_{x_c}(\Phi Q) + \nabla_{x_f}\{(1-\Phi)Q\} = 0 \quad (1)$$

$$\nabla_t Q + \nabla_{x_c}\left[\frac{\partial(\Phi Q)^2}{A_c}\right] + \nabla_{x_f}\left[\frac{\partial\{(1-\Phi)Q\}^2}{A_f}\right] + gA_c\left(S_c + \nabla_{x_c} z\right) + gA_f\left(S_f + \nabla_{x_f} z\right) = 0 \quad (2)$$

here,

$$\boldsymbol{\nabla_t \equiv \frac{\partial}{\partial t}},\ \boldsymbol{\nabla_{x_c} \equiv \frac{\partial}{\partial x_c}},\ \boldsymbol{\nabla_{x_f} \equiv \frac{\partial}{\partial x_f}},$$

here, A denotes cross-sectional area, Q discharge, S friction slope, z water depth, x distance along the flow direction, Φ the fraction of channel discharge, and t time. The model was developed using terrain data, river geometry, cross-sections, Manning's roughness, and design-flow boundary conditions. The rainfall trend series was not directly entered into HEC-RAS; instead, it provided a hydro-climatic context for interpreting flood susceptibility. The 25-, 50-, and 100-year scenarios were simulated using design discharge values derived from published hydrological information and return-period estimates. The source of different input data are given in Table 1. Model quality was checked through computational convergence, continuity of water-surface profiles, and consistency of simulated high-risk locations with reported flood-prone reaches. Because continuous observed water-level and discharge records were unavailable for all selected cross-sections, the outputs are interpreted as scenario-based flood susceptibility estimates rather than deterministic flood forecasts.

Table 1: Input Data for Numerical Simulation.

Input Data	Source
Terrain data of the study area	NASA SRTM Digital Elevation Model, 30 m spatial resolution (https://search.earth data.nasa.gov/search)
Projection file	https://spati alref erence.org/ref/sr-org/4691/
Flow data	Derived from published Farakka Barrage flow and barrage-regulated hydrology studies by Singh et al. [23] and Pal and Pani [24].

4 Results and Discussions

This section presents the rainfall trend results and the one-dimensional HEC-RAS simulations of water surface elevation, velocity, discharge, and inundation under different return-period scenarios.

4.1 Statistical Assessment of Long-Term Rainfall

Correlation Coefficient

Table 2 and Fig. 3 show that serial correlation was present before pre-whitening. At lags 1 and 10, ACF values were 0.405, and the Ljung–Box *p*-values were 0.0123 and 0.076, both below 0.05. After pre-whitening, the ACF values decreased to −0.082 at lag 1 and −0.360 & −0.361 at lag 3 and Lag 7, while Ljung–Box *p*-values increased to 0.4934 at lag 1 and 0.011, indicating that serial correlation was largely removed. Although the Box–Pierce result at lag 1 remained significant, the Ljung–Box test is more suitable for small samples and supports the use of pre-whitened series for subsequent trend analysis [2].

Table 2: Serial-correlation diagnostic results before and after pre-whitening.

Tests	Autocorrelation		Ljung-Box		Box-Pierce	
	Lag 1	Lag 10	Lag 1	Lag 10	Lag 1	Lag 10
Before Pre-Whitening	0.405	0.405	0.012	0.076	0.016	0.158
After Pre-Whitening	−0.082	−0.360, −0.361	0.493	0.011	0.511	0.052

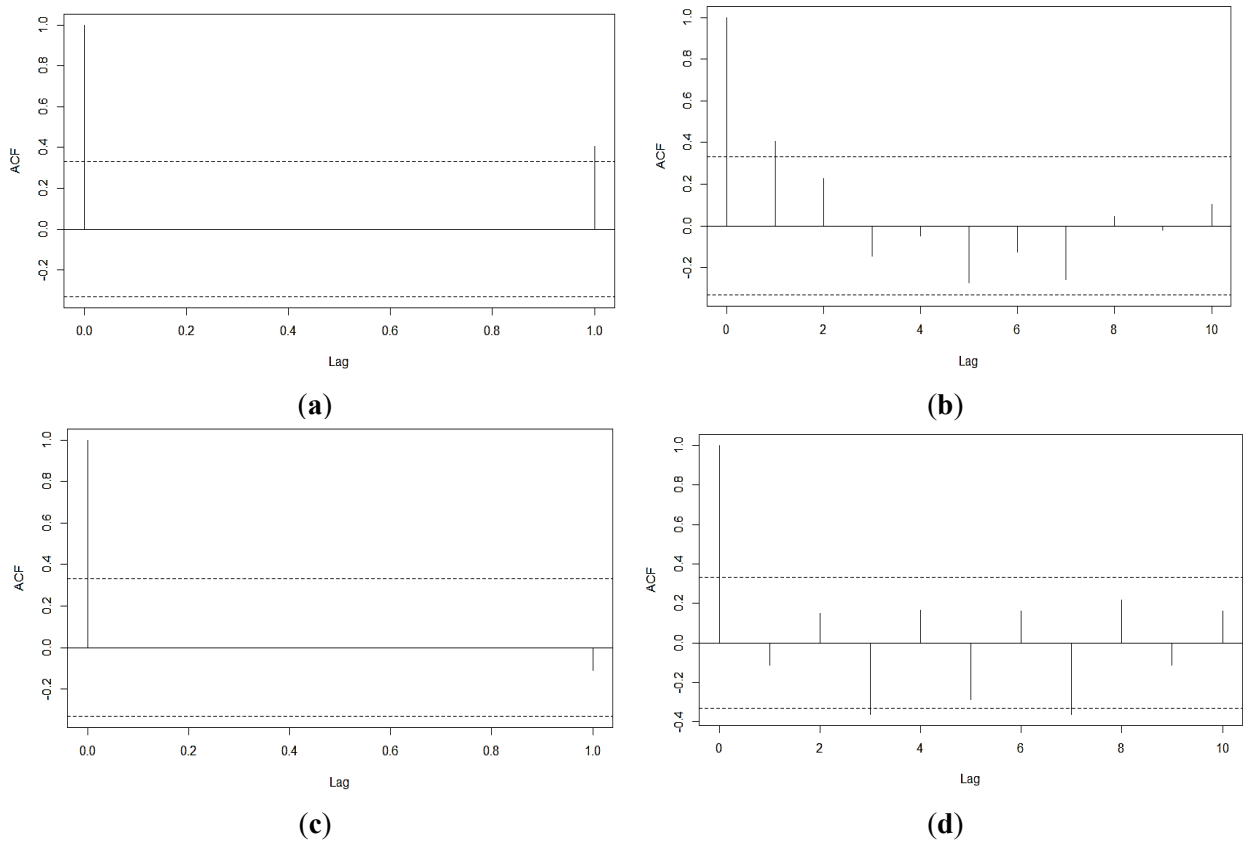

Figure 3: ACF plots for (**a**) lag 1 Before Pre Whitening, (**b**) lag 10 Before Pre Whitening, (**c**) lag 1 After Pre Whitening, (**d**) lag 10 After Pre Whitening.

Rainfall Trends

Table 3 presents Sen's slope estimates, and Fig. 4 compares the Z-values from different trend tests. A Z-value exceeding ±1.96 indicates significance at the 95% level, with negative values representing decreasing trends. Before pre-whitening, only MMKY showed a significant decreasing trend (Z = −2.69), while BCPW, TFPWMK, MK, and MMKH were non-significant (Z = −1.07 to −1.84). After pre-whitening, MMKH and MMKY showed significant decreasing trends, with Z-values of −2.83 and −2.73, respectively. Although BCPW, TFPWMK, and MK remained statistically non-significant after pre-whitening, all post-whitening Sen's slope estimates were negative, with MMKH and MMKY recording −0.1126 mm/year. Therefore, the rainfall series is interpreted as showing a decreasing tendency, with statistical significance mainly supported by the modified Mann–Kendall tests.

Table 3: Sen's slope estimates for annual rainfall trend analysis (mm/year)**.**

Tests	BCPW	TFPWMK	MK	MMKH	MMKY
Before Pre-Whitening	−0.0695	−0.1246	−0.0925	0.0650	0.0070
After Pre-Whitening	−0.0530	−0.0422	−0.0580	−0.1126	−0.1126

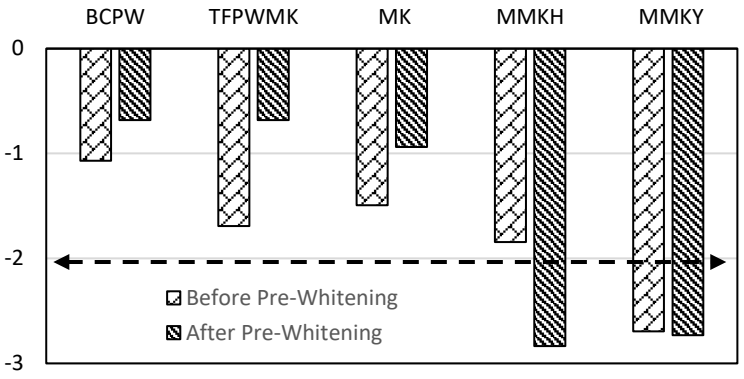

Figure 4: Comparison of results from multiple trend analysis techniques.

Identification of Trend Change Points

Table 4 summarises the Pettitt and SQMK change-point results. Before pre-whitening, Pettitt's test indicated a possible but statistically weak change point in 2020 (U* = 138; $p = 0.1499$). After pre-whitening, the probable change point shifted to 2021, but remained non-significant (U* = 100; $p = 0.513$), suggesting sensitivity to serial-correlation treatment. In SQMK, the intersection of the prograde and retrograde series indicates a possible trend shift, as shown in Fig. 5. SQMK identified an intersection in 2023 before and after pre-whitening, while early post-whitening intersections from 1992–1995 likely reflect minor fluctuations rather than meaningful shifts. Overall, Pettitt's test does not confirm an abrupt change point, whereas SQMK suggests a possible gradual rainfall shift around 2023.

Table 4: Results of trend change detection analysis.

Tests	Pettit	SQMK
Before Pre-Whitening	2020	2023
After Pre-Whitening	2021	1992, 1993, 1994, 1995, 2023

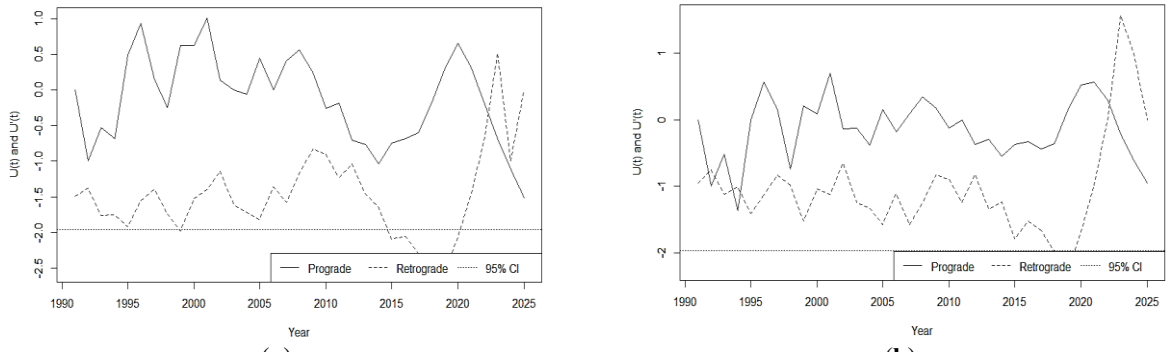

Figure 5: SQMK Plots (**a**) Before Pre-whitening (**b**) After Pre-whitening.

4.2 One-Dimensional Hydrodynamic Simulation

HEC-RAS 6.3 was used to simulate WSE, velocity, and discharge for 25-, 50-, and 100-year return-period scenarios. River stations were spaced at 5 km intervals along the 25 km reach, and 5 selected cross-sections out of the total 25 were used to examine spatial variation in channel geometry and hydraulic response.

Fig. 6 shows five selected cross-sections at RS 23,403, 20,069, 15,046, 10,055, and 5085, spaced at approximately 5 km intervals. The sections are irregular, with depths ranging from 15 m to 35 m, indicating

marked channel variability. RS 5085 shows a relatively narrow and steep profile, suggesting potential flow concentration during high discharges. Fig. 7 shows that WSE increases with return period and approaches riverbank elevations at several stations, particularly near RS 23,403. This indicates potential overtopping risk near critical infrastructure and highlights the need for flood-protection measures in vulnerable reaches [25, 26].

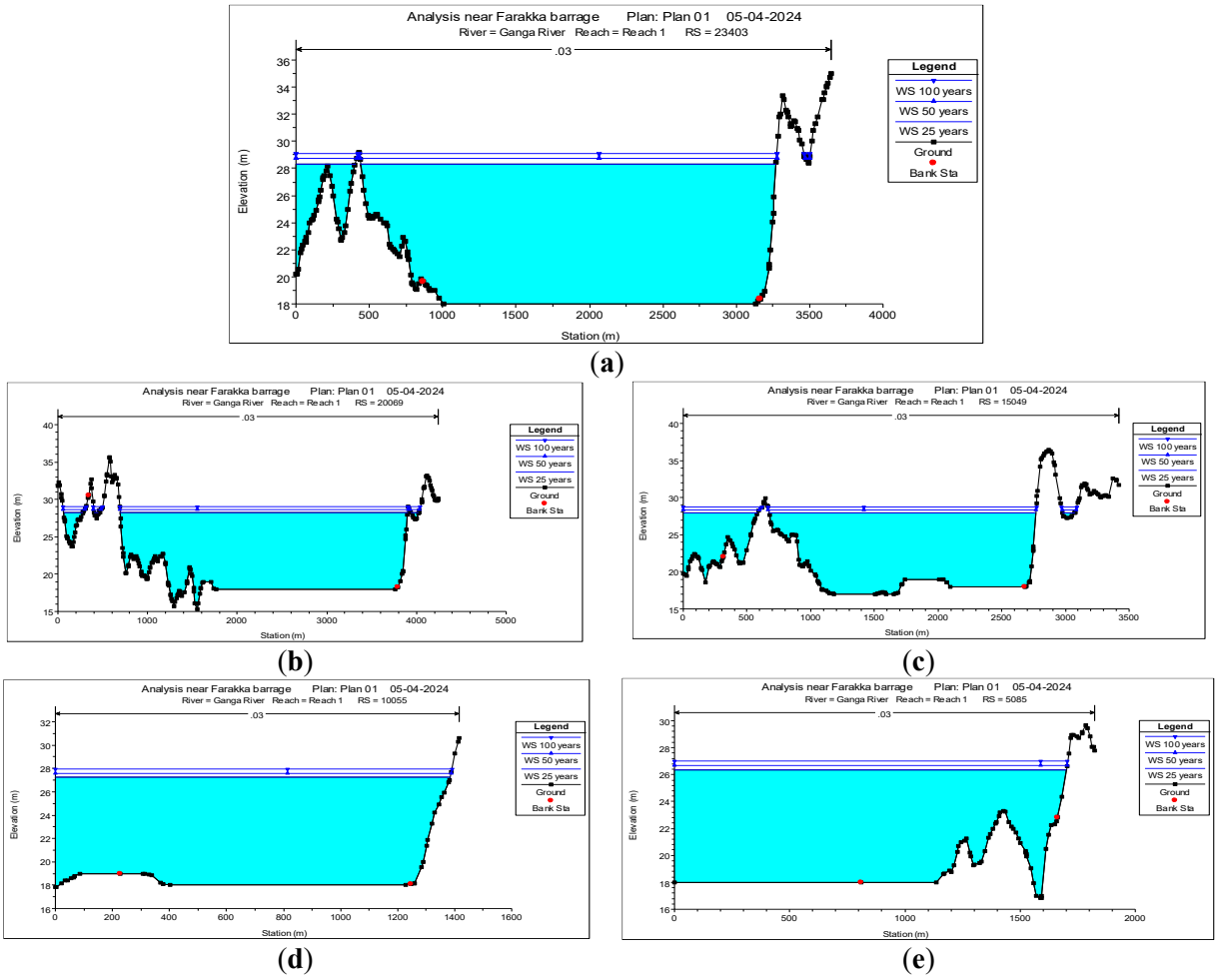

Figure 6: Simulated river cross section for RS (m): (**a**) 23,403, (**b**) 20,069, (**c**) 15,046, (**d**) 10,055, and (**e**) 5085.

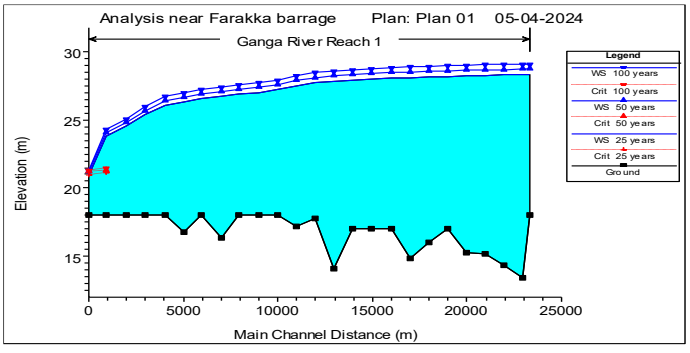

Figure 7: Simulated high flood level at the Farakka barrage location.

Fig. 8 illustrates the velocity distribution along the selected river channel for 25-year, 50-year, and 100-year return periods, with velocities ranging from 0.4 m/s to 5.7 m/s. Across all scenarios, a consistent pattern emerges. Velocity gradually increases in the downstream direction, suggesting energy concentration due to the narrowing of the channel. The highest velocities are observed near the left bank, approximately 2 km upstream of the downstream boundary, where the flow is intensified by channel constriction and asymmetrical geometry. These conditions lead to focused hydraulic forces, increasing the potential for bank erosion and channel scouring. As the return period lengthens, the magnitude of velocity rises correspondingly, intensifying erosion risks—particularly in areas lacking structural protection or natural resistance.

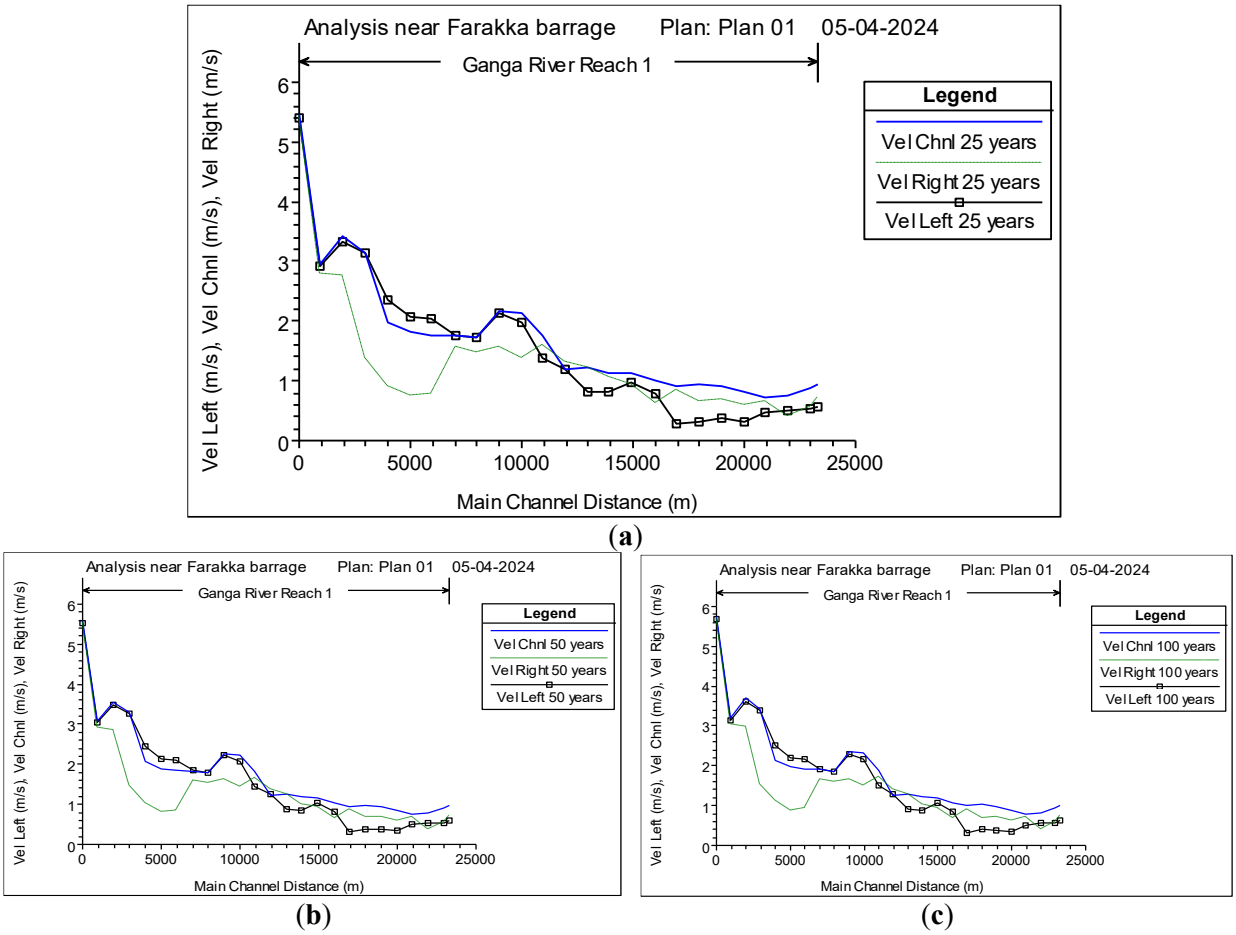

Figure 8: Velocity profiles for return periods of (**a**) 25 years, (**b**) 50 years, (**c**) 100 years.

Fig. 9 presents simulated discharge profiles across the same return periods. The discharge values range between 100 m^3/s and 24,000 m^3/s. The variation in discharge is nonlinear, indicating complex interactions between channel geometry, slope, and inflow volume. Unlike velocity, discharge does not follow a consistent spatial pattern but instead fluctuates due to local constrictions, floodplain interaction, and changing cross-sectional areas. As expected, the magnitude of discharge increases significantly from the 25-year to the 100-year scenario, with peak discharges recorded at locations with narrow channel widths and steep gradients. These high discharges amplify the risk of downstream flooding and stress the importance of early warning systems and discharge regulation, especially during extreme events.

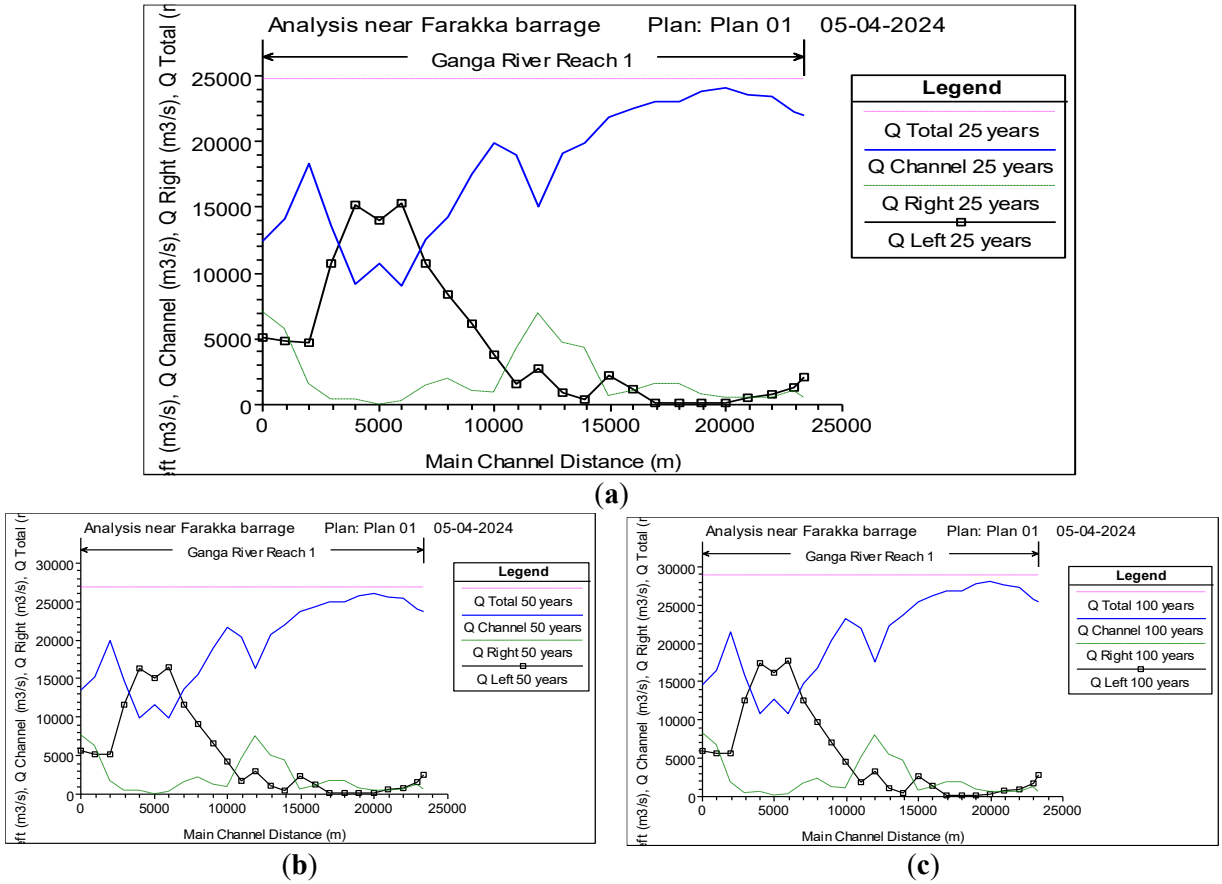

Figure 9: Discharge profiles for return periods of: (**a**) 25 years, (**b**) 50 years, and (**c**) 100 years.

Fig. 10 illustrates a bar chart representing the mean values of velocity and discharge, calculated using a numerical integration approach based on Eq. (3), as proposed by [27]:

$$p_m = \frac{\int_{x_{\min}}^{x_{\max}} p_x \; dx}{x_{\max} - x_{\min}} \tag{3}$$

where p_m is the mean value of the parameter p_x, while $x_{\max}$ and $x_{\min}$ are the maximum and minimum values of the channel distance x, respectively. The mean values of velocity (v_m) and discharge (Q_m) are derived accordingly. The bar chart is useful in analysing the flow characteristics and flood susceptibility in the study area.

Fig. 10 confirms that both velocity and discharge increase with longer return periods, consistent with expectations under higher flood scenarios. The increase in mean velocity and discharge reflects the amplified hydraulic response of the river system to intense rainfall events, thereby increasing the stress on riverbanks, embankments, and associated hydraulic structures. This visualisation helps synthesise and compare the overall flow characteristics, offering a clear representation of how the river's behaviour escalates with increasing flood risk.

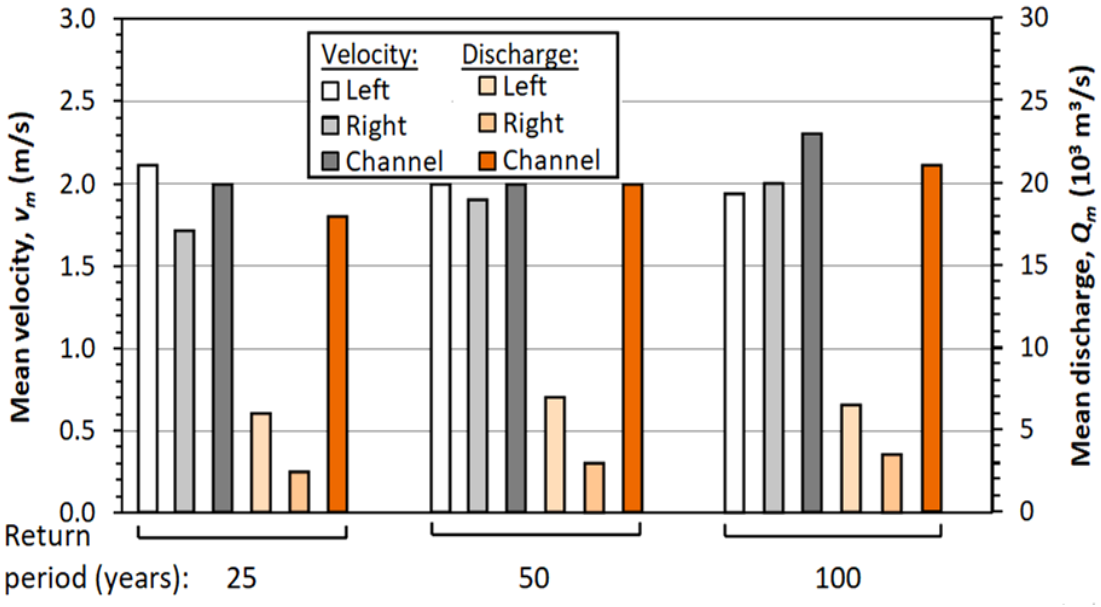

Figure 10: Bar chart of the mean values of velocity and discharge.

Fig. 11 shows the simulated flood inundation depth for the 25-, 50-, and 100-year return periods. Under the 25-year scenario, flood depths are mostly between 0 and 10 m and remain largely concentrated along the central channel and adjacent low-lying areas, although settlements such as Dhuliyan and Arjunpur may still experience localised flooding. In the 50-year scenario, flood depths increase to about 12 m and extend further into the floodplain, affecting areas such as Farakka Barrage Township and Mahadeb Nagar. Under the 100-year scenario, several reaches approach or exceed 15 m depth, with severe flood exposure around Lakshmipur, Chak Bahadurpur, Imamnagar, Nimtita, and Chachanda. These results indicate progressive expansion of flood depth and extent with increasing return period, increasing the risk of overtopping, erosion, and floodplain damage [13].

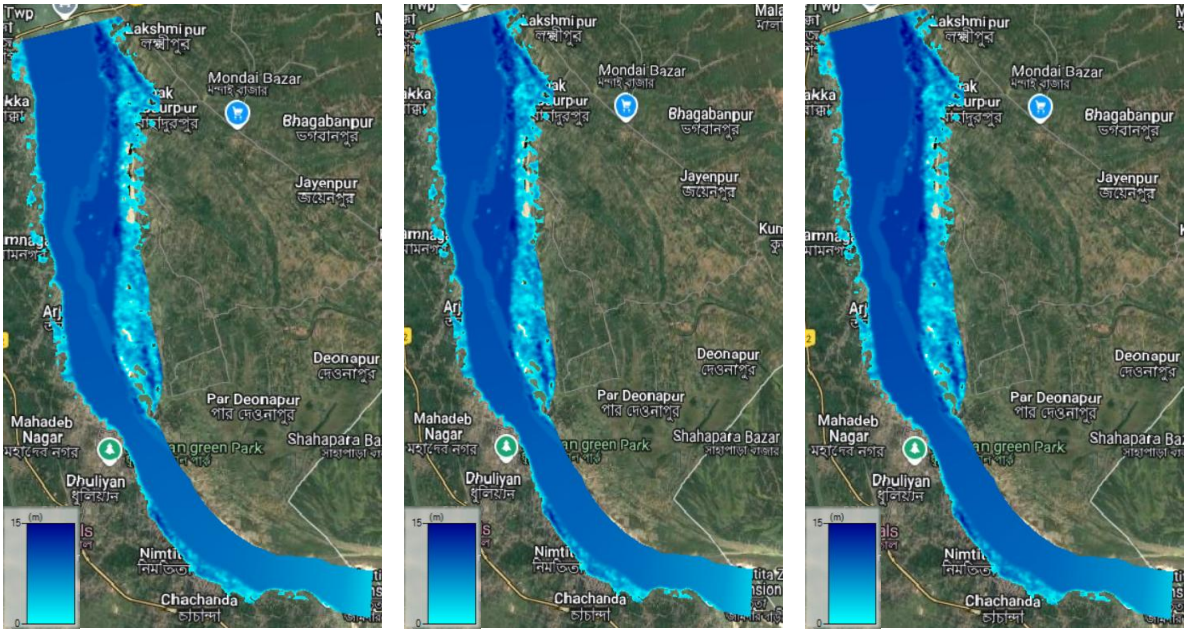

(**a**) (**b**) (**c**)

Figure 11: Flood inundation depth maps for return periods of (**a**) 25 years, (**b**) 50 years, and (**c**) 100 years.

Fig. 12 shows spatial velocity patterns for the 25-, 50-, and 100-year return periods. High-velocity zones are concentrated along the downstream left-bank reach, with flow speeds of about 10–15 m/s, while upstream areas near the Farakka Barrage show lower velocities, often below 3 m/s. The high-velocity area expands with return period, indicating increasing hydraulic stress under extreme flood scenarios. The downstream reach near Nimtita, Chachanda, and north of Pakur is therefore vulnerable to bank erosion, channel migration, sediment-transport imbalance, and possible embankment instability.

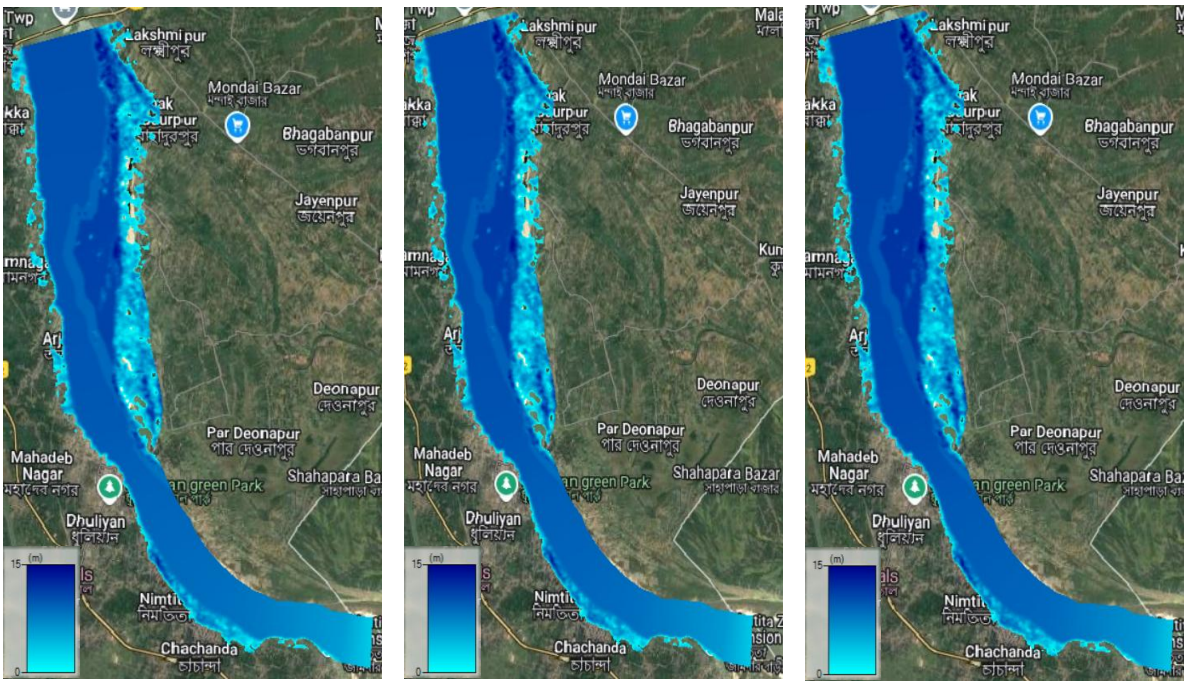

(**a**) (**b**) (**c**)

Figure 12: Flood inundation velocity maps for return periods of (**a**) 25 years, (**b**) 50 years, and (**c**) 100 years.

4.3 High-Risk Area

The high-risk zone map (Fig. 13) identifies the Farakka–Nimtita stretch as a vulnerable flood and erosion corridor. The yellow-shaded zone includes Chak Bahadurpur, Arjunpur, Mahadeb Nagar, Dhuliyan, and Nimtita. Here, sharp bends, narrow channels, mid-channel bars, low-lying settlements, and agricultural floodplain exposure coincide with high simulated flood depths and velocity concentrations. Additionally, the influence of the Farakka Barrage may contribute to elevated water levels upstream, intensifying backwater effects and reducing the channel's capacity to convey floodwaters efficiently. Densely populated areas like Dhuliyan and critical infrastructure near the riverbank, including transportation links and agricultural land, face considerable risk under 50- and 100-year return period flood scenarios. This combination increases the risk of inundation, bank erosion, and morphological instability, particularly under 50- and 100-year return-period scenarios. The results support targeted embankment strengthening, floodplain zoning, early-warning systems, and evacuation planning for the selected reach.

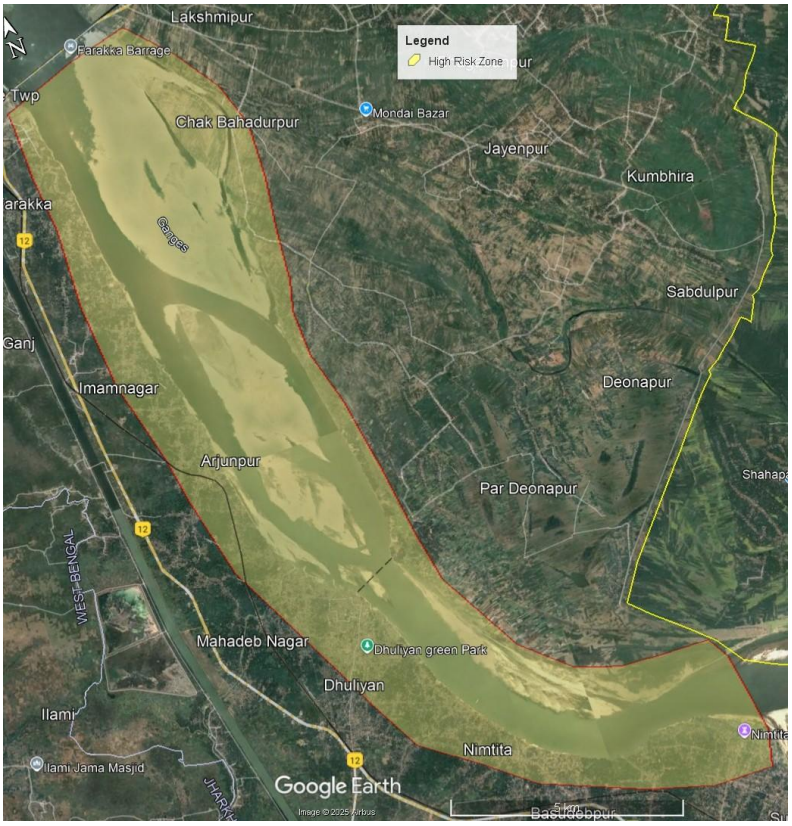

Figure 13: Identified high risk area.

5 Discussion

The rainfall trend analysis and hydrodynamic simulations should be interpreted as complementary rather than directly causal components. The statistical analysis indicates an overall decreasing annual rainfall trend, however, the significant decreasing trend was mainly detected by MMKH and MMKY, which are designed to account for serial correlation in hydrological time-series data. In contrast, the HEC-RAS simulations represent 25-, 50-, and 100-year design-flood scenarios and describe the hydraulic response of the river under high-magnitude flow conditions. Therefore, higher water surface elevation, velocity, and discharge under longer return periods do not contradict the decreasing annual rainfall tendency. Flood severity in the selected reach may also be affected by rainfall concentration during extreme events, upstream flow regulation, channel geometry, sedimentation, land-use change, and floodplain exposure. The SQMK indication around 2023 should be interpreted as a possible recent shift in rainfall behaviour, not as definitive evidence that flood hazard began in that year.

6 Significance of the Study

This study advances previous work by integrating rainfall trend diagnostics with site-specific one-dimensional hydraulic simulations for the selected reach near Farakka. Instead of examining rainfall variability or hydraulic response independently, the study jointly evaluates long-term rainfall tendency, change-point behaviour, channel geometry, design-flood hydraulics, and floodplain exposure. This integrated framework provides practical support for identifying priority reaches for embankment strengthening, zoning, and early-warning planning.

7 Conclusions

This study integrated long-term rainfall trend analysis and one-dimensional HEC-RAS modelling to assess hydro-climatic variability and flood susceptibility along the Ganga River downstream of the Farakka

barrage. The rainfall analysis, based on 34 years of daily data, indicated an overall decreasing annual rainfall tendency, although statistical significance was not consistent across all tests. The decreasing trend was mainly supported by the modified Mann–Kendall tests after accounting for serial correlation. Pettitt's test suggested statistically weak change points around 2020–2021, while SQMK indicated a possible trend shift around 2023. These results should be interpreted as evidence of gradual rainfall variability rather than abrupt hydrological change.

The HEC-RAS 6.3 simulations showed that WSE, velocity, discharge, and inundation extent increase under longer return-period flood scenarios. The Farakka–Nimtita reach, particularly near Dhuliyan, Arjunpur, and Nimtita, was identified as vulnerable because of high flow velocity, floodplain exposure, channel irregularity, and potential bank erosion. These locations should therefore be prioritised for embankment inspection, erosion-control measures, floodplain zoning, and early-warning planning.

Acknowledgement: The authors extend their appreciation to the Deanship of Research and Graduate Studies at King Khalid University for funding this work through Large Research Project under grant number RGP2/403/47. The infrastructure support is also received from Water Resources Department, Assam, Graphic Era Deemed to be University and North Eastern Regional Institute of Science and Technology.

Funding Statement: The work is funded through the Large Research Project, Deanship of Research and Graduate Studies at King Khalid University (grant number RGP2/403/47).

Author Contributions: The authors confirm contribution to the paper as follows: Conceptualization, Ghritartha Goswami, Majed Alsubih and Sudip Basack; Methodology, Ghritartha Goswami, Majed Alsubih, Saiful Islam and Sudip Basack; Resources, Ghritartha Goswami, Majed Alsubih, Saiful Islam and Sudip Basack; Software, Ghritartha Goswami and Pranjit Borah; Data curation, Ghritartha Goswami and Pranjit Borah; Validation, Ghritartha Goswami and Pranjit Borah; Formal analysis, Ghritartha Goswami and Pranjit Borah; Funding, Majed Alsubih; Project administration, Majed Alsubih and Saiful Islam; Writing – original draft, Ghritartha Goswami and Sudip Basack; Writing-revising, Ghritartha Goswami, Majed Alsubih, Saiful Islam, Sudip Basack and Pranjit Borah. All authors reviewed and approved the final version of the manuscript.

Availability of Data and Materials: Data will be made available upon reasonable request.

Ethics Approval: Not applicable.

Conflicts of Interest: The authors declare no conflicts of interest.

References

1. Salaeh, N., Ditthakit, P., Pinthong, S., Hasan, M. A., Islam, S., Mohammadi, B., & Linh, N. T. T. (2022). Long-short term memory technique for monthly rainfall prediction in Thale Sap Songkhla river basin, Thailand. Symmetry, 14(8), 1599. https://doi.org/10.3390/sym14081599
2. Goswami, G., & Prasad, R. K. (2023a). Trend analysis of rainfall pattern in Arunachal Pradesh (India). Environmental Modeling and Assessment. https://doi.org/10.1007/s10666-023-09903-3
3. Touseef, M., Chen, L., Yang, K., & Chen, Y. (2020). Long-term rainfall trends and future projections over Xijiang River Basin, China. Advances in Meteorology. https://doi.org/10.1155/2020/6852148
4. Aznarez, C., Jimeno-Sáez, P., López-Ballesteros, A., Pacheco, J. P., & Senent-Aparicio, J. (2021). Analysing the impact of climate change on hydrological ecosystem services in Laguna del Sauce (Uruguay) using the SWAT model and remote sensing data. Remote Sensing, 13(10). https://doi.org/10.3390/rs13102014
5. Farhangi, M., Kholghi, M., & Chavoshian, S. A. (2016). Rainfall trend analysis of hydrological subbasins in western Iran. Journal of Irrigation and Drainage Engineering, 142(10), 05016004. https://doi.org/10.1061/(ASCE)IR.1943-4774.0001040
6. Sarma, B., Sarma, A. K., & Singh, V. P. (2013). Optimal ecological management practices (EMPs) for minimizing the impact of climate change and watershed degradation due to urbanization. Water Resources Management, 27(11), 4069–4082. https://doi.org/10.1007/s11269-013-0396-y

7. Gajbhiye, S., Meshram, C., Singh, S. K., Srivastava, P. K., & Islam, T. (2016). Precipitation trend analysis of Sindh River Basin, India from 102-year record (1901–2002). Atmospheric Science Letters, 17(1), 71–77. https://doi.org/10.1002/asl.602
8. Ghosh, A., Roy, M. B., & Roy, P. K. (2020). Estimation and prediction of the oscillation pattern of meandering geometry in a sub-catchment basin of Bhagirathi-Hooghly River, West Bengal, India. SN Applied Sciences, 2(9), 1–24. https://doi.org/10.1007/s42452-020-03275-z
9. Mubialiwo, A., Abebe, A., Kawo, N. S., Ekolu, J., Nadarajah, S., & Onyutha, C. (2022). Hydrodynamic modelling of floods and estimating socio-economic impacts of floods in Ugandan river Malaba sub-catchment. Earth Systems and Environment, 6, 45–67. https://doi.org/10.1007/s41748-021-00283-w
10. Samanta, S., Dalai, T., Tiwari, S., & Rai, S. (2018). Quantification of source contributions to the water budgets of the Ganga (Hooghly) River estuary, India. Marine Chemistry, 207. https://doi.org/10.1016/j.marchem.2018.10.005
11. Singh, R. K., Villuri, V. G. K., Pasupuleti, S., & Nune, R. (2020). Hydrodynamic modeling for identifying flood vulnerability zones in lower Damodar River of eastern India. Ain Shams Engineering Journal, 11(4), 1035–1046. https://doi.org/10.1016/j.asej.2020.01.011
12. Goswami, G., Prasad, R. K., & Kumar, D. (2023a). Hydrodynamic flood modeling of Dikrong River in Arunachal Pradesh, India: A simplified approach using HEC-RAS 6.1. Modeling Earth Systems and Environment. https://doi.org/10.1007/s40808-022-01507-2
13. Goswami, G., & Prasad, R. K. (2023b). Hydrodynamic flood modeling with HEC-RAS 6.3: A case study of the Pakke River in Siejosa, Arunachal Pradesh, India. In S. Ahmad & R. Murray (Eds.), World Environmental & Water Resources Congress 2023 (pp. 261–270). ASCE. https://doi.org/10.1061/9780784484852.025
14. Hassan, A. B. M. E. (2019). Indian hegemony on water flow of the Ganges: Sustainability challenges in the southwest part of Bangladesh. Sustainable Futures, 1, 100002. https://doi.org/10.1016/j.sftr.2019.100002
15. Goswami, G., Mandal, S., Basack, S., Mukherjee, R., & Karakouzian, M. (2023b). Assessing the impacts of land use and land cover changes on the water quality of river Hooghly, West Bengal, India: A case study. Hydrology, 10(71). https://doi.org/10.3390/hydrology10030071
16. Das, B., Pal, S. C., & Malik, S. (2018). Assessment of flood hazard in a riverine tract between Damodar and Dwarkeswar River, Hugli District, West Bengal, India. Spatial Information Research, 26, 91–101. https://doi.org/10.1007/s41324-017-0157-8
17. Porwal, V., & Choudhary, M. P. (2023). Investigating variations and trend analysis for temperature and precipitation as a result of climate change in Rajasthan, India. Journal of Climate Change, 9(3), 33-40. https://doi.org/10.3233/JCC230022
18. Akthar, Z., Jan, B., Zehra, S., & Inayatullah, S. (2026). Study the Temporal Variability of Climate Change in Urban City Karachi, Pakistan. Journal of Climate Change. 11. 23. 10.70917/jcc-2025-033.
19. Kowalczuk, Z., Świergal, M., & Wróblewski, M. (2018). River flow simulation based on the HEC-RAS system. In J. M. Kościelny et al. (Eds.), Advanced Solutions in Diagnostics and Fault Tolerant Control. Advances in Intelligent Systems and Computing (Vol. 635). Springer. https://doi.org/10.1007/978-3-319-64474-5_21
20. Pettitt, A. N. (1979). A non-parametric approach to the change-point problem. Journal of the Royal Statistical Society: Series C (Applied Statistics), 28(2), 126–135. https://doi.org/10.2307/2346729
21. U.S. Army Corps of Engineers (USACE). (1998). HEC-1 Flood Hydrograph Package User's Manual. Hydrologic Engineering Center, Davis, California.
22. U.S. Army Corps of Engineers (USACE). (2024). HEC-RAS software downloads. https://www.hec.usace.army.mil/software/hecras/downloads.aspx
23. Singh, U., Desai, V. R., Sharma, P. K., & Ojha, C. S. P. (2022). Simulating pre-monsoon and post-monsoon flows at Farakka Barrage, India. Sustainable Water Resources Management. https://doi.org/10.1007/s40899-021-00594-w.
24. Pal, R., & Pani, P. (2016). Seasonality, barrage (Farakka) regulated hydrology and flood scenarios of the Ganga River: A study based on MNDWI and simple Gumbel model. Modeling Earth Systems and Environment, 2, 57. https://doi.org/10.1007/s40808-016-0114-x.
25. Kumar, N., Lal, D., Sherring, A., & Issac, R. K. (2017). Applicability of HEC-RAS and GFMS tool for 1D water surface elevation/flood modeling of the river: A case study of river Yamuna at Allahabad (Sangam), India. Modeling Earth Systems and Environment, 3(4), 1463–1475. https://doi.org/10.1007/s40808-017-0390-0
26. Pathan, A. I., & Agnihotri, P. G. (2021). Application of new HEC-RAS version 5 for 1D hydrodynamic flood modeling with special reference through geospatial techniques: A case of river Purna at Navsari, Gujarat, India. Modeling Earth Systems and Environment, 7(2), 1133–1144. https://doi.org/10.1007/s40808-020-00961-0
27. Basack, S., Goswami, G., & Nimbalkar, S. (2021). Analytical and numerical solutions to selected research problems in geomechanics and geohydraulics. WSEAS Transactions on Applied and Theoretical Mechanics, 16, 222–231. https://doi.org/10.37394/232011.2021.16.25